Journal of Materials Chemistry A

PAPER

View Article Online
View Journal

Cite this: DOI: 10.1039/c8ta01986j

Flexible cellulose nanopaper with high wet tensile strength, high toughness and tunable ultraviolet blocking ability fabricated from tobacco stalk *via* a sustainable method†

Qingbo Wang, ‡[ab] Haishun Du, ‡[ad] Fang Zhang,[c] Yuedong Zhang,[a] Meiyan Wu,[a] Guang Yu,[a] Chao Liu, *[a] Bin Li *[a] and Hui Peng[a]

Cellulose nanopaper (CNP) is of great interest to researchers mainly due to its renewability, excellent mechanical properties and optical properties. However, CNP is usually sensitive to water, resulting in the loss of strength and durability. To overcome this issue, in this work, an efficient and sustainable route, which involved ammonium sulfite cooking and formic acid hydrolysis, was reported to isolate lignin-containing cellulose nanofibrils (CNFs) from tobacco stalk. The resultant CNFs were directly used to fabricate strong, flexible, and water resistant CNP without any complex chemical modification. The residual lignin was found to act as a reinforcing agent between CNFs in CNP. The tensile strength and toughness of the lignin-containing CNP (255 MPa and 19.7 MJ m^{-3}) were much higher compared with those of the one without lignin (179 MPa and 12.8 MJ m^{-3}). The water-resistance of the CNP was also improved extraordinarily, and its maximum wet tensile strength reached up to 83 MPa which is the highest value in comparison with the reported CNP. Compared to the lignin-free CNP, the lignin-containing CNP also showed the better thermal stability and excellent UV-blocking properties. The present work designed a new route to prepare lignin-containing CNFs and CNP, which are potential candidates to replace petroleum-based materials in many advanced applications.

Received 2nd March 2018
Accepted 13th April 2018

DOI: 10.1039/c8ta01986j

rsc.li/materials-a

Introduction

With increasing concern about environmental issues and the overexploitation of fossil resources, people have been developing biodegradable materials from biomass to substitute the traditional petroleum-based materials. As an inexhaustible polymer mainly generated from plants, cellulose has been paid much attention over the past decades, particularly for cellulose nanofibrils (CNFs), which are relatively new and renewable one-dimensional nanomaterials.

CNFs can be used to prepare cellulose nanopaper (CNP) which exhibits many desirable properties such as high mechanical strength, excellent optical properties, good thermostability, low thermal expansion, and low oxygen permeability.[1] Therefore, CNP has been considered as a promising sustainable material for use in the fields of electronic devices,[2] visual display substrates,[3] batteries,[4] *etc.*

However, CNP is sensitive to moisture due to the hydrophilic nature of cellulose. Absorption of moisture could weaken the interfibrillar hydrogen bonding and cause swelling, resulting in the loss of strength and durability. These drawbacks limited the usability of CNP under high-moisture environments or in water.[5]

Substituting the hydrophilic hydroxyl groups of cellulose with hydrophobic functional groups is a way to overcome this obstacle. Acetylation,[6] silylation,[7] esterification[8] and polymer grafting[9] have been conducted for this purpose. However, these processes often suffer from low efficiency and hazardous chemicals or time-consuming processes, which hindered their commercial application. Moreover, chemical modifications could also damage the original crystal structure of CNFs, reducing the mechanical and barrier properties of the resultant CNP.[10] Forming covalent or non-covalent bonding between the CNF surface and other substances, such as phenolic resins,[11] hydrophobic silica,[12] *etc.*, is another strategy to enhance the water resistance of CNP. Though the resultant composite CNP could exhibit excellent properties, the introduction of expensive

[a]CAS Key Laboratory of Bio-based Material, CAS Key Laboratory of Biofuels, Qingdao Institute of Bioenergy and Bioprocess Technology, Chinese Academy of Sciences, Qingdao, Shandong, 266101, China. E-mail: liuchao@qibebt.ac.cn; libin@qibebt.ac.cn

[b]Faculty of Modern Agricultural Engineering, Kunming University of Science and Technology, Kunming, 650504, China

[c]National Engineering Research Center for Nanotechnology, Shanghai, 200241, China

[d]Department of Chemical Engineering, Auburn University, Auburn, AL 36849, USA

† Electronic supplementary information (ESI) available. See DOI: 10.1039/c8ta01986j

‡ Both authors contributed equally.

building blocks or complicated procedures was unavoidable for its fabrication.

Most of the previous studies focused on lignin-free CNFs for CNP production. The mechanical properties of CNP are directly affected by the interfibrillar hydrogen bonds within CNP. Lignin can hinder the hydrogen bonding and usually causes reduction of mechanical strength.[13] Also, lignin is a random network polymer located in the cell wall of natural plants and it works as a joining material which binds the other components (*e.g.*, cellulose and hemicelluloses) together. Therefore, the presence of lignin was also considered to be able to increase the mechanical properties of CNP by the binding effect.[14,15] But the reinforcing effect of lignin is usually hindered and counteracted by its hydrophobic nature, which interferes with hydrogen bonding between the CNFs in CNP. However, achieving a significant improvement of mechanical properties by introducing lignin is still theoretically possible. Furthermore, owing to the rich aromatic groups and complex structure, lignin could serve as a natural hydrophobic agent,[16] plasticization agent[17] and UV-absorbent[18] by interacting with the polymeric matrix or other nanoparticles. Therefore, it is expected that retaining lignin in CNFs could not only generate multiple or synergistic functions of the final products, but also simplify the processing and lower the processing cost.

Cellulose fibers are usually extracted by traditional alkaline or acid cooking followed by a bleaching step to facilitate the subsequent fabrication of CNFs. Methods including acid hydrolysis, TEMPO-mediated oxidation, high-pressure homogenization, high-intensity ultrasonication, or enzyme-assisted hydrolysis have been adopted to produce CNFs.[19] The morphology and properties of CNFs were different depending on the chosen method and raw materials.[20] However, the drawbacks of huge water usage, chemical recycle problems and liquid waste disposal need to be well addressed. Hence, the development of a sustainable and clean approach is of significant importance for the production of CNFs, particularly for large-scale applications.

Ammonium sulfite cooking is a good substitute method for the pretreatment of lignocellulose. The spent liquor of ammonium sulfite cooking can be used as fertilizers as reported previously.[21] Formic acid (FA) hydrolysis is a sustainable and economical approach for CNF production because FA could be easily recycled *via* evaporation. Also, esterification and hydrolysis of cellulose could be achieved in a one-pot reaction of FA treatment. The introduced ester groups can be used to adjust the polarity and hydrophilicity of the CNF surface. A high yield of 70–90% for CNFs could be achieved and no dialysis was needed, which could dramatically reduce the water consumption and production cost.[22]

On the other hand, CNFs can be fabricated from cellulosic materials like wood and agricultural waste.[23] Tobacco is a special and important economic crop all over the world. In China, 1.5 million tons of tobacco stalk (TS) are produced annually, and are generally burnt as trash in the field after the marketable leaves are harvested, which causes severe air pollution and waste of materials with a high content of cellulose.[24] Therefore, high-value utilization of TS is worthy of concern.

In this work, TS was subjected to ammonium sulfite cooking followed by FA hydrolysis plus homogenization to prepare CNFs. Different treatment conditions were used to tune the lignin contents (0–13.7%) of CNFs. After homogenization, the obtained CNFs were used to prepare CNP through a simple filtration procedure (Fig. 1). The surface properties, mechanical strength, barrier properties and optical properties of the prepared CNP were fully characterized, and the mechanisms of

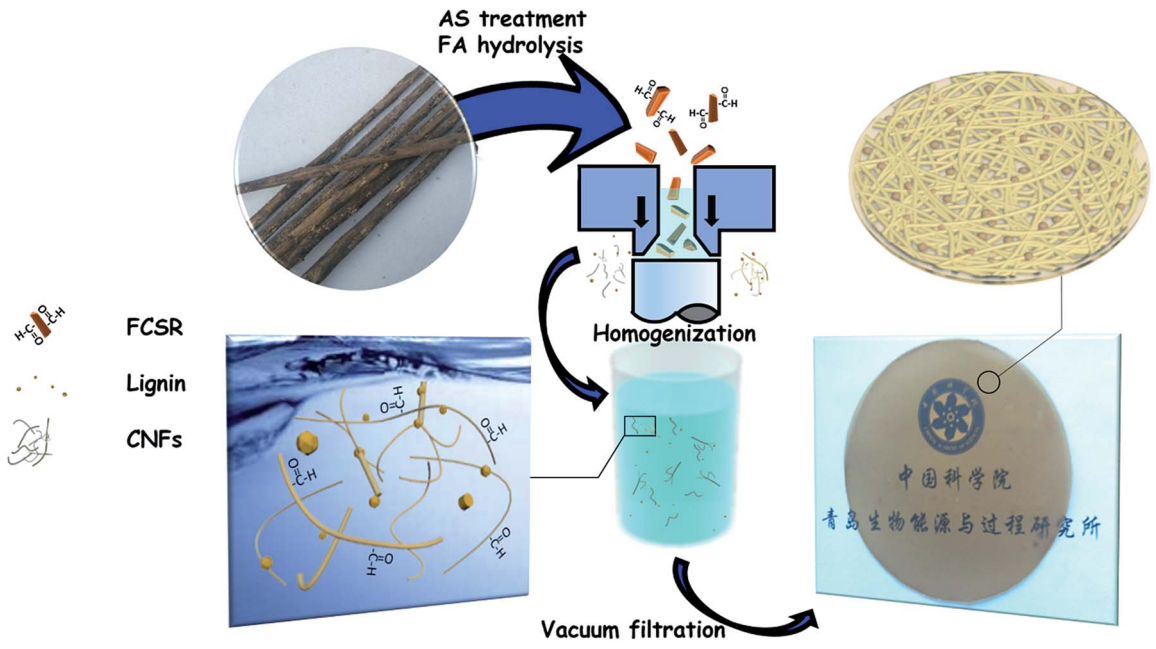

Fig. 1 Schematic diagram of the preparation of lignin-containing CNP.

the enhanced mechanical properties (particularly for the super high wet strength and toughness) of the resultant CNP containing lignin were also discussed. This work provides a new and sustainable route for the production of CNP containing lignin. The prepared CNP with excellent toughness, wet strength and UV blocking ability will have many promising and advanced applications.

Experimental

Materials

Raw TS (Weifang, China) was peeled to eliminate roots and barks, and then smashed under 20 mesh. Ammonium sulfite (90%) was purchased from MACKLIN (Shanghai, China). Urea (99%) was obtained from Beijing Solarbio Science & Technology Co., Ltd. FA (88 wt%), hydrogen peroxide (H_2O_2, 30 wt%), sodium hydroxide (NaOH), and dimethylacetamide (DMAC) were purchased from Sinopharm Chemical Reagent Co., Ltd. 2,2,6,6-Tetramethylpiperidine-1-oxyl (TEMPO, 98 wt%) and sodium hypochlorite (active chlorine 14 wt%) were bought from Aladdin Reagents (Shanghai, China).

Methods

Ammonium sulfite pretreatment. Ammonium sulfite cooking was carried out at 160 °C for 2 h using a rotating reactor system (VRD-42SD-A, China National Pulp and Paper Research institute, Ltd.). The TS powder was treated with 10, 15 and 20% of ammonium sulfite charge (based on the oven dried mass of TS) to achieve different levels of delignification. The dosage of urea was 6% on the basis of the oven dried mass of TS for each cooking to maintain weak alkali conditions. The cooked TS samples (named 10AT, 15AT and 20AT, respectively) were collected by filtration and washed with deionized water until pH reached neutral.

In order to obtain the lignin-free sample, 20AT was bleached with 5% H_2O_2 (based on the oven dried mass of 20AT) at 90 °C for 2 h. The liquid-to-solid weight ratio was 10 and the pH of the mixture was 10.5 by adjusting with 1 M NaOH solution. This whole process was repeated 3 times until the snowy-white bleached sample (referred to as BT) was obtained.

Preparation of CNFs. Raw TS, AT and the bleached BT samples were dried at 75 °C for 4 h. Then, FA hydrolysis was conducted to further break down the above samples (each trial processed 6 g sample) and release lignin. TS was directly treated with FA (1 : 30, w/v) with 300 rpm mechanical stirring at 95 °C for 6 and 8 h, respectively. The FA hydrolyzed solid residue (FCSR) was rinsed with FA to remove the dissolved substances and then rinsed with water to neutralize the pH. The resultant FCSRs containing 13.7 and 12.3 wt% residual lignin were named 14F and 12F, respectively. AT and BT samples were treated with FA (1 : 30, w/v) with 300 rpm mechanical stirring at 95 °C for 6 h, respectively. The obtained FCSR was also rinsed with FA and water to remove impurities. The resultant FCSRs containing 10.3, 5.8, 3.4 and 0.1 wt% residual lignin were named 10F, 6F, 3F and 0F, respectively. The remaining water in FCSR was removed by centrifugation and solvent exchange with DMAC (thrice), and then the FCSR was homogenized at a concentration of 4 wt% in DMAC. The CNFs containing different amounts of lignin (named 14-CNFs, 12-CNFs, 10-CNFs, 6-CNFs, 3-CNFs and 0-CNFs) were obtained after passing through an ATH-BASIC homogenizer (ATH Engineering Limited, China) 3 times at 30 MPa and then 5 times at 100 MPa. TEMPO-mediated oxidized CNFs (TO-CNFs) were prepared for comparison according to the previous methods.[25]

Preparation of CNP. CNF suspensions were diluted to 0.2 wt% with DMAC. 110 mL of diluted suspension was used to fabricate CNP by vacuum filtration using a filter membrane (diameter of 10 cm, pore size of 0.44 μm, polypropylene). The resulting wet CNP was placed between two filter membranes and dried under vacuum at 70 °C for 3 h. The obtained CNPs were named 14-CNP, 12-CNP, 10-CNP, 6-CNP, 3-CNP and 0-CNP according to their lignin contents. The CNP made from TO-CNFs (TO-CNP) was fabricated in water, following the same method as mentioned above.

Characterization

The chemical compositions of the samples were determined following the National Renewable Energy Laboratory procedure.[26] A scanning electron microscope (SEM, Hitachi S-4800) was employed to observe the morphologies of the treated TS and the cross-section of CNP. The morphologies of CNFs were obtained *via* a transmission electron microscope (TEM, Hitachi H-7600) and an atomic force microscope (AFM, Agilent 5400), respectively. The surface roughness of CNP was analysed using the AFM with a scanning speed of 0.6 line per s in the tapping mode. The crystallinity index (CrI) of each pulp and CNP sample was measured using an X-ray diffractometer (XRD, Bruker Discover D8). The range of the scattering angle (2θ) was from 5 to 40° with a scan rate of 4° min^{-1} at 40 kV and 40 mA. Fourier transform infrared spectroscopy (FTIR) spectra of TS, pulp and CNF samples were recorded on an FTIR spectrometer (Nicolet 6700, Thermo Fisher Scientific Inc.) from 4000 to 400 cm^{-1} at a resolution of 4 cm^{-1}. The thermal stability of CNF and CNP samples were evaluated using a thermogravimetric analyzer (METTLER TGA/DSC1). The temperature was increased from 30 to 600 °C at a heating rate of 10 °C min^{-1} under nitrogen (25 mL min^{-1}) protection. The tensile strength of the CNP samples was measured using a universal testing machine and determined following the TAPPI standard method (TAPPI T497 and TAPPI T456). The initial distance between the two clamps of the tester was 20 mm and tensile deformation was performed at 5 mm min^{-1}. Before the wet tensile strength test, CNP samples were pre-soaked in water for 24 h. 5 measurements were carried out for each sample and the average was reported. The toughness of CNP was calculated as the area under the stress–strain curve. The rate of water vapor permeability (RWVP) was measured following the ASTM E96A procedure. Oxygen permeability (OP) was measured using a PERME-OX2/230 analyzer (Labthink). The surface interaction between deionized water and the CNP was measured using an AST VCA Optima XE contact angle analyser (AST Products). At least 3 areas were measured on each sample. The UV-Vis transmittance

of each CNP was measured using a spectrophotometer with an integrating sphere (U-4100 HITACHI). The haze was measured using a haze meter (NDH-5000, Nippon Denshoku Industries Co. Ltd.) following the method of ISO 14762-1999.

Results and discussion

Chemical characterization

The chemical compositions of TS and cellulose samples are shown in Table S1.† The adoption of ammonium sulfite cooking aimed to open up the wood structure, remove the noncellulosic components and sulfonate the lignin. Different degrees of delignification were obtained by adjusting the ammonium sulfite dosage. After ammonium sulfite cooking, the lignin contents of the obtained 10AT, 15AT and 20AT samples were 21.7, 15.6 and 14.0%, respectively. The remaining lignin in BT (0.1%) almost vanished after bleaching. Subsequently, the samples of raw TS, 10AT, 15AT, 20AT and BT were hydrolyzed with FA, respectively. After FA hydrolysis, hemicellulose in all samples was almost totally removed (Table S1†). Moreover, lignin was further removed during FA treatment. The obtained FCSR samples had gradually decreasing lignin contents of 13.7, 12.3, 10.3, 5.8, 3.4 and 0.1%.

The chemical components of the samples were also investigated by FTIR, as shown in Fig. S1.† The samples show similar spectra, which were typical cellulose structural characteristics.[27] The peaks at 1739, 1508 and 1225 cm^{-1} could be only observed in TS. They were assigned to C=O and C=C aromatic skeletal vibrations and guaiacyl units in lignin, respectively.[28–30] The band at 1720 cm^{-1} corresponded to the C=O stretching vibration indicating the presence of ester groups after FA treatment.[31,32]

Morphology

SEM images of the TS, 20AT, BT, 14F, 3F and 0F are shown in Fig. S2.† As can be observed in Fig. S2a,† the fibers of TS are aggregated together in a rather large size. After ammonium sulfite cooking and bleaching (Fig. S2b and S2c†), the structures of 20AT and BT were cracked. This was mainly owing to the removal of lignin and hemicellulose, which act like cross-linking agents in TS fibers. These destructed and cracked structures could allow FA to get into the inner part more rapidly, therefore facilitating the subsequent defibrillation and delignification. As shown in Fig. S2d–f,† most of the fiber bundles were defibrillated into individual fibers and some of the fibers were destructed into smaller fragments after FA hydrolysis. Compared to 3F and 0F, 14F exhibited a minimum level destruction possibly owing to the fact that the remaining lignin inhibited the FA hydrolysis.[33]

TEM images of CNFs are shown in Fig. 2. The width of 14-CNFs ranged from 5 to 50 nm. 3-CNFs were more homogeneous, and their width ranged from 5 to 30 nm. Owing to the nearly complete delignification of bleaching, 0-CNFs were more uniform and smaller in diameter. Their width ranged from 5 to 15 nm. A similar phenomenon could be observed in the AFM images (Fig. 3). 14-CNFs mainly consisted of fibers with a height

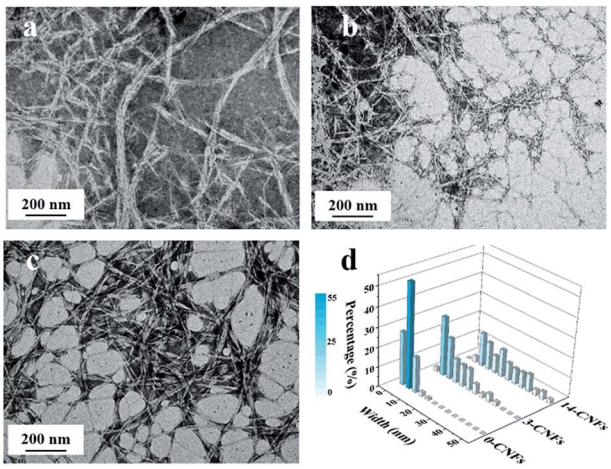

Fig. 2 TEM images of (a) 14-CNFs, (b) 3-CNFs, (c) 0-CNFs and (d) width distribution of 14-CNFs, 3-CNFs and 0-CNFs.

(diameter) of 50 nm and a few fibers were 20 nm in height, while most of the 3-CNFs were less than 20 nm in height and very few fibers were over 30 nm in height. Owing to the effective delignification, the height of 0-CNFs was mainly around 5 nm with a few fibers over 15 nm in height, and they were more homogeneous in both shape and size.

XRD

Compared to amorphous hemicellulose and lignin, cellulose has a more distinct crystalline structure mainly owing to the strong hydrogen bonding and van der Waals interactions.[34] The crystallinity of cellulose is crucial to its mechanical and thermal properties.[35] The CrI of CNFs and CNP samples was analyzed by XRD to gain further insights into the structural changes and the results are summarized in Fig. 4 and S3.† The main diffraction peaks were at around $2\theta = 15.1°$, 17.5°, 22.7° and 34.3°, corresponding to (1−10), (110), (200) and (004) diffraction planes,

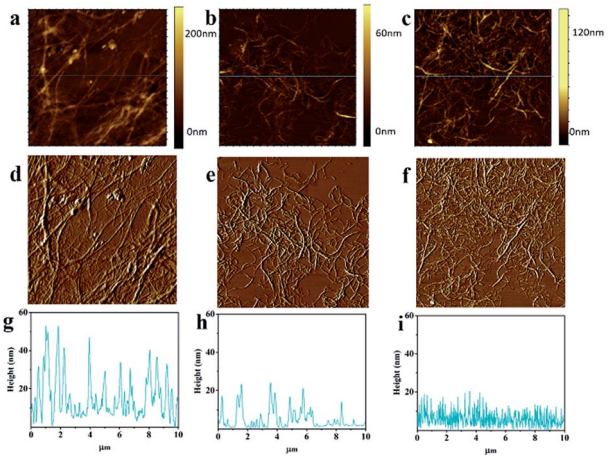

Fig. 3 AFM height images (a–c), phase images (d–f) and height profiles (g–i) of 14-CNFs (a, d, and g), 3-CNFs (b, c, and h) and 0-CNFs (c, f, and i).

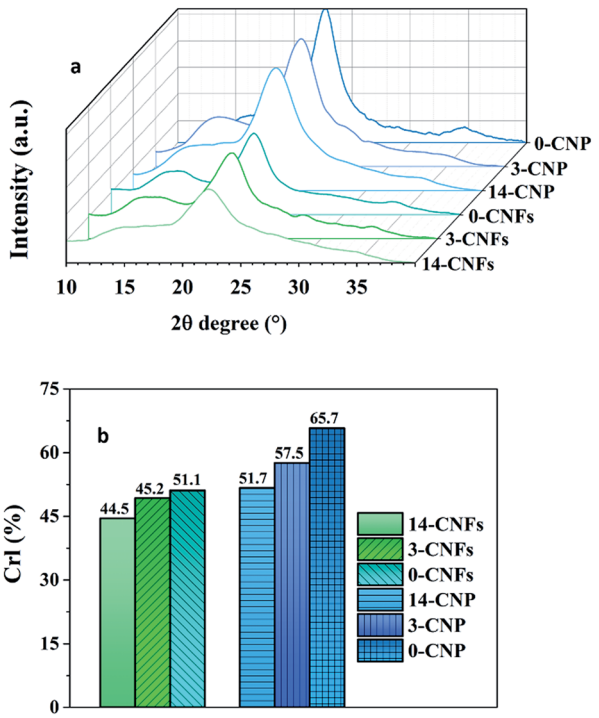

Fig. 4 XRD pattern (a) and CrI (b) of CNF and CNP samples.

which are the typical patterns of cellulose I.[36] The result indicated that the chemical and mechanical treatment did not change the crystal type of cellulose.

The CrI of the TS increased after cooking and bleaching treatment, as displayed in Fig. 4b and S3.† The increase of CrI was mainly due to the removal of amorphous components (*e.g.* lignin and hemicelluloses), which was consistent with the composition analysis as indicated in Table S1.† After FA hydrolysis, the CrI of the samples increased due to the further degradation of lignin, hemicellulose and amorphous regions of cellulose. A decrease of CrI could be observed after the homogenization process. For instance, the CrI of 3F was 64.7%, whereas the CrI decreased to 45.2% (3-CNFs). This was mainly due to the fact that part of the crystalline domains of cellulose was damaged by high shear force during the high-pressure homogenization process.[37] Interestingly, the CrI of the samples increased after CNP formation. The solubility of the cellulose derivative in organic solvents was related to the degree of substitution.[38] It was reported that the surface layer of modified CNFs could be dissolved in solvents with ball milling.[6] It could be supposed that part of the CNFs can be dissolved in DMAC with the assistance of mechanical force when a certain degree of substitution of ester groups was achieved during FA hydrolysis. This might be another reason why the CrI decreased during the homogenization process. The dissolved cellulose could be regenerated and form a crystalline structure from DMAC/LiCl solutions.[39] A similar experimental phenomenon was observed in this study. The CrI of all CNF samples increased after the drying process of CNP (Fig. 4b). The transition from amorphous form to crystalline cellulose might enhance the barrier and thermal properties of CNP. Moreover, the partial dissolution of CNFs, caused by the introduction of ester groups and mechanical treatment, could also have a positive effect on the mechanical properties of CNP. The regeneration of dissolved cellulose could form a more continuous phase and establish more connections between CNFs. Then, the stress could transfer better and the pull-out of CNFs would require more energy, which have an important impact on the enhancement of the tensile strength and toughness of the obtained CNP.

Thermal stability

Thermal gravimetric (TG) and derivative thermogravimetric (DTG) curves are presented in Fig. S4.† The onset temperature of thermal decomposition (T_{on}) and maximum decomposition temperature (T_{max}) are referred to as the beginning and maximum rate of degradation temperature, respectively, which are summarized in Table S2.†

The T_{on} of TS was 290 °C. After ammonium sulfite cooking and bleaching, the T_{on} of both 20A and BT increased to approximately 310 °C owing to the partial removal of noncellulosic substances.[40] After FA hydrolysis, FCSR samples also showed an enhancement in thermal stability. The T_{on} of 14F, 3F and 0F increased to 345, 341.5 and 338 °C, respectively. This was mainly owing to the further removal of hemicellulose as during the FA hydrolysis process. FA hydrolysis could also destroy the amorphous region of cellulose and lead to an improvement in crystallinity which benefited the increase of thermal stability. Moreover, the thermostability of the sample improved with the increase of residual lignin content.[41] However, the thermal stability of FCSR samples showed a considerable decline after the homogenization process. The T_{on} of 14-CNFs, 3-CNFs and 0-CNFs decreased to 308, 304 and 299 °C, respectively. This decrease of thermal stability was because the homogenization destroyed part of the crystalline region of cellulose, thus leading to a decrease of the crystallinity of CNF samples. On the other hand, after the homogenization process, the increasing surface area made CNFs more likely to be degraded when they are exposed to heat. The T_{on} of 14-CNP, 3-CNP and 0-CNP increased to 333, 326 and 317 °C, as shown in Table S2.† This was mainly due to the improved crystallinity after regeneration,[42,43] as indicated in Fig. 4.

Mechanical properties of CNP

The mechanical properties of CNP are essential for its applications. After the homogenization, the CNFs exhibited good dispersibility in DMAC (Fig. S5†). Well dispersed CNFs would help form a more uniform structure, which could benefit the mechanical performance of the resulting CNP. The densities and tensile properties of CNP samples with different lignin contents are listed in Table S1.† The densities of the CNP samples were in the range of 1.30–1.33 g cm^{-3} with a thickness of 33 ± 3 μm. Systematic dependencies between the lignin content and density were observed in some studies.[15] In this study, the densities of CNP were not significantly different at the 97% level and independent of the lignin content. The possible reason was that part of the residual lignin filled the voids

among the CNFs in the dry CNP.[14] The sticky lignin could adhere to the CNFs and act as a binder, which might severely affect the tensile properties of CNP. Excellent mechanical properties, such as high strength and toughness, are required for the most advanced material design. However, the enhancements of strength and toughness are usually conflicted.[44] Strength represents the material's resistance to non-recoverable deformation. Toughness is the material's resistance to fracture (deformability) and measured by the area under the stress–strain curve. Materials with high toughness possess the ability to dissipate local high stress through enduring deformation. Improvement of strength is often associated with the loss of toughness and the material tends to be more brittle. Achieving both high strength and high toughness often requires a complicated and expensive preparation process.[44] The lignin-containing CNP usually exhibits poor or comparable mechanical properties, compared with the ones from fully bleached pulp fibers, and the preservation of lignin is usually unable to significantly improve the tensile performance of CNP.[14] In this study, we found that the residual lignin had clear improvement effects on the tensile strength and toughness.

The strain–stress curves of CNP are shown in Fig. 5a and the detailed mechanical property values are summarized in Table 1.

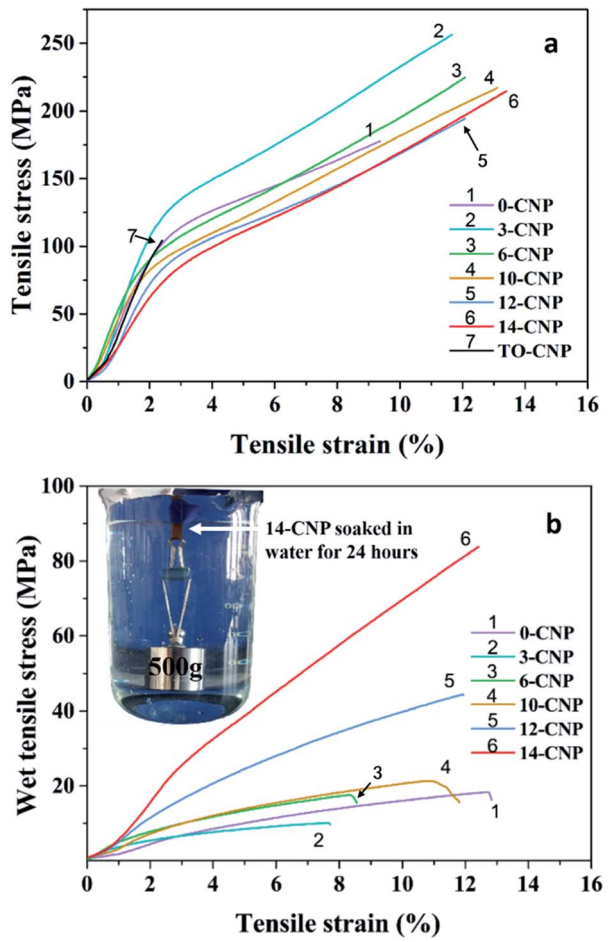

Fig. 5 Dry (a) and wet (b) strain–stress curves of CNP samples with different lignin contents.

In the presence of lignin, the strength and toughness of CNP increased simultaneously. The strength and toughness of the lignin-free sample (0-CNP) are 179.2 ± 5.5 MPa and 12.8 ± 1.9 MJ m^{-3}, respectively. 3-CNP with 3.4 wt% residual lignin exhibited the best mechanical performance of 255.2 ± 18.8 MPa and 19.7 ± 3.8 MJ m^{-3} among the CNP samples. Accordingly, this is about 42% and 54% higher compared to the lignin-free sample (0-CNP), respectively. Especially, the toughness of 3-CNP (19.7 MJ m^{-3}) is 10.94 and 19.7 times higher than those of natural nacre and steel (1.8 and 1.0 MJ m^{-3}), respectively.[45] The lignin could interfere with the formation of hydrogen bonding between CNFs and consequently brought about a negative impact on tensile strength. On the other hand, a small amount of lignin could aid stress-transfer between CNFs and thus enhance the tensile performance.[14] Fig. 5a also shows that further increasing the lignin contents would cause a gradual and slight decrease of tensile strength. The strength and toughness decreased from 255.2 ± 18.8 MPa and 19.7 ± 3.8 MJ m^{-3} to 215.7 ± 5 MPa and 17.0 ± 0.8 MJ m^{-3}, respectively, when the lignin content increased from 3.4 to 13.7 wt%. Too much lignin would interfere with the formation of intermolecular hydrogen bonding and thereby cause a slight decrease of mechanical properties. In this study, the presence of lignin in the CNP could lead to the simultaneous improvement of strength and ductility.

The size of CNFs also has an important impact on the mechanical properties of CNP. Decreasing the diameter of CNFs could reduce the defects of CNP, and achieve better strength and toughness simultaneously.[44] As shown in Fig. 2d, the diameter of 0-CNP (5–15 nm) was smaller than that of 3-CNP (5–30 nm). It was expected that the smaller diameter led to a stronger CNP, but this effect was counteracted by the distribution of lignin in 3-CNP. The existence of lignin could improve the mechanical performance of CNP. Yet, excess residual lignin could not only interfere with the hydrogen bonding, but also increase the diameter of CNFs, thus further decreasing the strength and toughness. Hence, the larger diameter might be another reason why the mechanical properties of 14-CNP (diameter of 5–50 nm) decreased.

In addition, SEM cross-section images of CNP (Fig. 6 and S6†) showed that the nanofibers were organized into laminar structures. Clearly, the layer structures of all CNP samples were very close except 12-CNP and 14-CNP. The loose structure of 12-CNP and 14-CNP might be owing to the fact that the residual lignin particles in 12-CNP and 14-CNP were not sulfonated, and these relatively big lignin particles interfered with the hydrogen bonding between CNFs. The tensile stress and Young's modulus of CNP investigated in this study were compared with others reported in the literature, and the results are shown in Fig. 7. These reported CNP samples were fabricated from fully bleached CNFs or lignin-containing CNFs. The lignin-containing CNP in the present study exhibited high tensile strength and low Young's modulus. The elongation at break of CNP was improved by the retention of lignin. The elongation at break of the lignin-free sample was about 9.6% (0-CNP). When the residual lignin was involved, the elongation at break reached 11.4% (3-CNP) and increased with the increase of lignin

Table 1 Physical properties of CNP

Sample	Tensile strength[a]	Toughness[b]	Young's module[c]	Wet tensile strength[d]	Density[e]	ROP[f]	RWVP[g]
0-CNP	179.2 ± 5.5	12.8 ± 1.9	5.0 ± 0.9	18.0 ± 0.5	1.32 ± 0.13	1.88×10^{-12}	3.15×10^{-3}
3-CNP	255.2 ± 18.8	19.7 ± 3.8	6.4 ± 1.1	9.7 ± 1.2	1.31 ± 0.05	2.05×10^{-12}	2.76×10^{-3}
6-CNP	222.7 ± 11.3	17.5 ± 3.1	5.7 ± 0.4	17.6 ± 4.2	1.33 ± 0.01	2.67×10^{-12}	3.28×10^{-3}
10-CNP	217.6 ± 11.6	17.5 ± 0.6	5.5 ± 0.5	19.8 ± 1.3	1.30 ± 0.11	2.80×10^{-12}	2.57×10^{-3}
12-CNP	192.4 ± 9.4	14.4 ± 2.7	5.0 ± 0.6	44.3 ± 2.3	1.31 ± 0.07	1.15×10^{-8}	2.87×10^{-3}
14-CNP	215.7 ± 5.0	17.0 ± 0.8	4.6 ± 0.9	83.5 ± 12	1.31 ± 0.05	1.45×10^{-8}	3.08×10^{-3}
TO-CNP	104.3 ± 4.3	1.3 ± 0.2	6.4 ± 1.8	ND[h]	ND	ND	ND

[a] Tensile strength of CNP (MPa). [b] Toughness of CNP (MJ m^{-3}). [c] Young's module of CNP (GPa). [d] Wet tensile strength of CNP (MPa). [e] Density of CNP (g cm^{-3}). [f] Rate of oxygen permeability, RH = 50% (cm^3 cm cm^{-2} s cmHg). [g] Rate of water vapor permeability, RH = 50% (g per day per m per kPa). [h] ND: not determined.

content. The increase in elongation at break with the lignin content was related to the sticky and soft nature of lignin. This improvement of elongation at break led to a relatively low Young's modulus. Compared to TO-CNP (elongation at break of 2.4%) fabricated from TEMPO-medium oxidized CNFs and CNP prepared in other studies (Fig. 7), these lignin-containing CNP fabricated in this study exhibited an obvious advantage in the aspect of ductility.

Wet strength and water resistance of CNP

Fig. 5b shows the wet mechanical properties of the CNP immersed in water for 24 h. After immersion, the CNP swelled up and its thickness increased from 33 ± 3 to 55 ± 5 μm. Under wet conditions, the water molecules can break the hydrogen bonds between CNFs and then lead to swelling and deterioration of mechanical strength. The presence of lignin on the CNP surface and the lignin filling the void between the CNFs could act as a barrier for water penetration and thus maintained the tensile strength. Ammonium sulfite cooking introduced sulfonic groups on lignin molecules and increased the hydrophilicity of the residual lignin which was retained in the obtained CNP.[57] A higher amount of hydrophilic lignin could not effectively increase the wet strength of the CNP. As shown in Fig. 5b, the tensile strength of 0-CNP, 3-CNP, 6-CNP and 10-CNP fell below 20 MPa (from 9.7 to 19.8 MPa), when the CNP was wetted with water. Without ammonium sulfite cooking, the wet strengths of 12-CNP and 14-CNP, containing approximately 12 and 14% unsulfonated lignin, reached 44.3 ± 2.3 and 83.5 ± 12 MPa, respectively. 14-CNP (thickness 55 μm, width 10 mm) could lift a weight of 500 g in water (see the video in the ESI†). Lignin was more hydrophobic, and covered the surface of the CNFs. A high amount of hydrophobic lignin can shield the accessible hydroxyl groups, reducing the formation of hydrogen bonding with water molecules and thus enhancing the water-resistance of CNP.

The contact angle was measured to characterize the surface wettability of CNP as shown in Fig. S7.† FA hydrolysis could reduce the amount of surface hydroxyl groups, but the resultant CNP still remained hydrophilic. The contact angle of CNP gradually increased with the increase of lignin contents (in the range of 0 to 10%) due to the hydrophobicity of lignin.[58] Some of the surface hydroxyl groups on CNFs were substituted by hydrophobic ester groups, but the contact angle of 0-CNP (61.2°) was still similar to the one of TO-CNP (62.0°), probably due to the abundant hydroxyl groups. Then, a sharp increase of

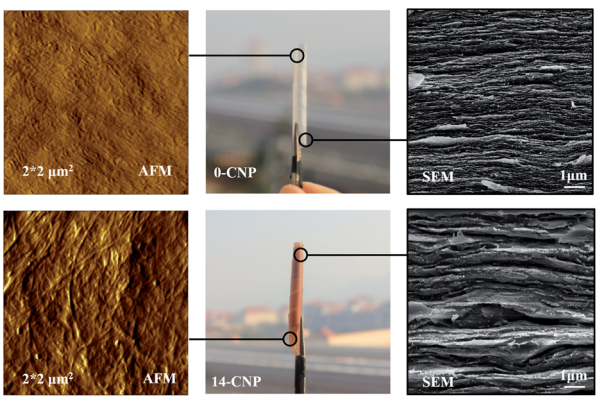

Fig. 6 AFM surface images of 0-CNP and 14-CNP (left), rolled up 0-CNP and 14-CNP (middle) and SEM cross-section images of 0-CNP and 14-CNP (right).

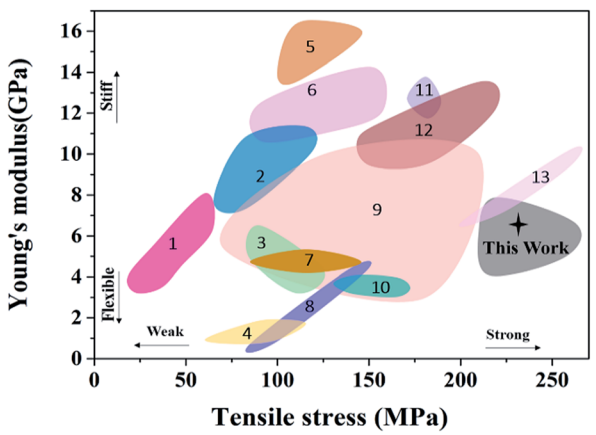

Fig. 7 Tensile stress and Young's modulus map to compare CNP prepared by using different materials and methods. (1)[46] Bagasse, (2)[47] bleached kraft hardwood, (3)[48] algae, (4)[49] softwood sulphite pulp, (5)[50] MFC, (6)[47] bleached kraft hardwood, (7)[51] corncob, (8)[52] softwood sulfite pulp, (9)[53] KC Flock W-50, (10)[54] rice straw, (11)[55] bleached sulfite softwood, (12)[56] softwood dissolving pulp, and (13)[44] kraft bleached softwood.

the contact angle was observed when the lignin content increased from 10 to 13.7%. Sulfonation during ammonium sulfite cooking made the lignin more hydrophilic and affected the surface properties of lignin-containing CNP.[59] Without ammonium sulfite cooking, the presence of lignin can build more hydrophobic surfaces and therefore the highest contact angle of 90.1° (14-CNP) was obtained. Thus, the hydrophilicity or hydrophobicity of the residual lignin can also affect the surface wettability of the resulting CNP.

To further demonstrate the water resistant properties, the TS CNP samples fabricated from FA treated CNFs and TEMPO oxidized CNFs were immersed in water (Fig. S8†). It was found that TO-CNP was deconstructed within 3 days, while 0-CNP fabricated using the FA-treated CNFs could keep its shape even after 100 days, despite the similar contact angles of TO-CNP and 0-CNP. As discussed in the section of XRD, after FA hydrolysis, the surface layer of CNFs could be partly dissolved with the assistance of mechanical force. During the drying process, the dissolved part could be regenerated, fill the voids in the dry CNP and then form a more compact structure, thus enhancing the water resistance of 0-CNP. Therefore, the CNP prepared using the FA-treated CNFs exhibited good water resisting properties.

Barrier properties of CNP

The barrier properties of CNP are summarized in Table 1. The oxygen barrier properties were slightly reduced with the increase of residual lignin when the lignin content was below 10%. The ROP of 0-CNP was 1.88×10^{-12} cm^3 cm cm^{-2} s cmHg and it increased to 2.80×10^{-12} cm^3 cm cm^{-2} s cmHg for 10-CNP. This might be owing to the increased crystallinity of CNP, because a higher degree of crystallinity leads to better oxygen and water vapour barrier properties.[60] The ROP increased drastically to 1.15×10^{-8} and 1.45×10^{-8} cm^3 cm cm^{-2} s cmHg for 12-CNP and 14-CNP, respectively. This might be owing to the loose structure as shown in Fig. S6.† The RWVP of CNP was nearly around 3×10^{-3} g per day per m per kPa. It did not show a linear dependence on the lignin content or degree of crystallinity, because RWVP was mostly influenced by its density.[61]

Optical properties of CNP

Transparency, UV-blocking and haze are important optical properties for CNP. The UV-Vis light transmittance of CNP samples is displayed in Fig. 8. For illustrating the optical performance of these CNPs intuitively, the transmittance of ultraviolet A, ultraviolet B and visible light [T(Vis), T(UVA) and T(UVB)] was calculated using the equations reported previously, respectively.[62] The UV-blocking performance is shown in Fig. 9.

It could be clearly seen in Table S3† that the transmittance of lignin-free CNP ranked first among all optical spectra with 87.27, 80.68 and 76.34% (for T(Vis), T(UVA), and T(UVB), respectively). As for the CNP with lignin, the transparency in all UV-Vis spectra showed a considerable decline and this trend got more severe with the increase of residual lignin. This phenomenon corresponded to the UV absorption spectrum, and the absorption got more intense with higher lignin content. When the lignin content was 3.4%, T(Vis), T(UVA) and (UVB)

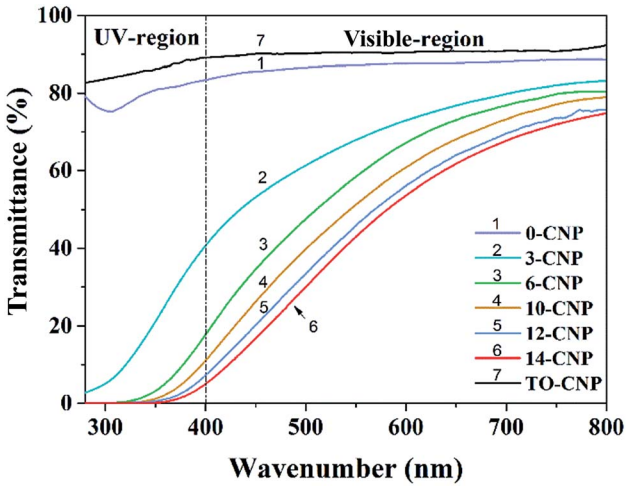

Fig. 8 UV transmittance of CNP samples.

decreased to 69.64, 24.35 and 4.94%, respectively. When the lignin content reached 13.7%, T(Vis), T(UVA) and (UVB) were 48.14, 1.05 and 0.03%, respectively. The CNP with lignin content above 5.8% exhibited over 93% absorption of UVA and full UVB absorption. This remarkable UV absorbing performance was attributed to the chemical construction of lignin. Lignin possesses lots of UV-absorbing functional groups such as phenolic units, ketones and other chromophores, which make it a natural broad-spectrum blocker.[63] Mechanical properties of CNP are important for different applications. Although the retained lignin offers UV-blocking properties to the CNP, it also usually brings the drawback of deteriorating the mechanical properties of the conventional CNP.[18] In the present work, lignin acted as a reinforcing agent in CNP, and the UV absorption and tensile strength of CNP improved

Fig. 9 UV-blocking performance of CNP samples. Paper money was shielded by nothing, 0-CNP, 10-CNP and 14-CNP, respectively, and then exposed to UV light (LED, 10 cm in height, wavenumber of 365 nm).

simultaneously. Moreover, both lignin-free and lignin-containing CNP exhibited relatively high optical haze, as shown in Table S3 and Fig. S9.† The retained lignin led to an increased diameter of nanofibers, which could generate high light scattering and haze.[64] Therefore, the haze of CNP increased with the increase of lignin contents. The UV absorption and haze of CNP could be adjusted to some extent by controlling the lignin content. The obtained CNP has potential applications in optoelectronic devices, such as solar cells.

Conclusions

In this paper, lignin-containing CNFs were prepared by a sustainable method *via* ammonium sulfite cooking followed by FA hydrolysis and the effects of lignin content on the properties of CNFs and CNP were investigated. The tensile strength and toughness of CNP were improved up to 255.2 MPa and 19.7 MJ m^{-3} simultaneously with the residual lignin (3.4 wt%) which acted as a binder just like in natural wood. A high lignin content of 13.7 wt% provided a significant improvement in the wet tensile strength (83.5 MPa) and contact angle (90.1°) of CNP. The wet strength and surface wettability of CNP could also be influenced by the hydrophilicity or hydrophobicity of the residual lignin. Furthermore, the residual lignin could impart a better thermal stability to the resultant CNP compared to the lignin-free CNP. In the meantime, the lignin could act as a UV-blocker and enable the CNP to absorb UV. In summary, the retained part of lignin not only can lead to a lower production cost by reducing the use of chemicals and a simplified process, but also can enhance the mechanical, thermal, water-resistant and UV absorbing performances of the obtained CNP. These characteristics of CNP demonstrated its potential use in the fields of energy storage, high quality packaging, electronics, *etc.*

Conflicts of interest

There are no conflicts to declare.

Acknowledgements

This work was financially supported by the National Natural Science Foundation of China (No. 31470609, No. 25106240 and No. 31700509), the Primary Research and Development Plan of Shandong Province (No. 2016CYJS07A02), as well as the "Transformational Technologies for Clean Energy and Demonstration", Strategic Priority Research Program of the Chinese Academy of Sciences (No. XDA21060201). In addition, H. D. acknowledges the financial support from the China Scholarship Council.

Notes and references

1 D. Klemm, F. Kramer, S. Moritz, T. Lindstrom, M. Ankerfors, D. Gray and A. Dorris, *Angew. Chem., Int. Ed.*, 2011, **50**, 5438–5466.
2 F. Hoeng, A. Denneulin and J. Bras, *Nanoscale*, 2016, **8**, 13131–13154.
3 X. Xu, J. Zhou, L. Jiang, G. Lubineau, T. Ng, B. S. Ooi, H. Y. Liao, C. Shen, L. Chen and J. Y. Zhu, *Nanoscale*, 2016, **8**, 12294–12306.
4 J. Sheng, S. Tong, Z. He and R. Yang, *Cellulose*, 2017, **24**, 4103–4122.
5 A. J. Benitez, J. Torres-Rendon, M. Poutanen and A. Walther, *Biomacromolecules*, 2013, **14**, 4497–4506.
6 S. Deng, R. Huang, M. Zhou, F. Chen and Q. Fu, *Carbohydr. Polym.*, 2016, **154**, 129–138.
7 K. Missoum, M. Belgacem and J. Bras, *Materials*, 2013, **6**, 1745–1766.
8 S. X. Peng, H. Chang, S. Kumar, R. J. Moon and J. P. Youngblood, *Cellulose*, 2016, **23**, 1825–1846.
9 M. Hakalahti, A. Salminen, J. Seppala, T. Tammelin and T. Hanninen, *Carbohydr. Polym.*, 2015, **126**, 78–82.
10 A. Hambardzumyan, L. Foulon, N. B. Bercu, M. Pernes, J. E. Maigret, M. Molinari, B. Chabbert and V. Aguié-Béghin, *Chem. Eng. J.*, 2015, **264**, 780–788.
11 W. Yang, H. Bian, L. Jiao, W. Wu, Y. Deng and H. Dai, *RSC Adv.*, 2017, **7**, 31567–31573.
12 D. Le, S. Kongparakul, C. Samart, P. Phanthong, S. Karnjanakom, A. Abudula and G. Guan, *Carbohydr. Polym.*, 2016, **153**, 266–274.
13 K. L. Spence, R. A. Venditti, O. J. Rojas, Y. Habibi and J. J. Pawlak, *Cellulose*, 2010, **17**, 835–848.
14 E. Rojo, M. S. Peresin, W. W. Sampson, I. C. Hoeger, J. Vartiainen, J. Laine and O. J. Rojas, *Green Chem.*, 2015, **17**, 1853–1866.
15 A. Ferrer, E. Quintana, I. Filpponen, I. Solala, T. Vidal, A. Rodríguez, J. Laine and O. J. Rojas, *Cellulose*, 2012, **19**, 2179–2193.
16 H. Bian, Y. Gao, R. Wang, Z. Liu, W. Wu and H. Dai, *Cellulose*, 2018, **25**, 1–10.
17 J. Bouajila, P. Dole, C. Joly and A. Limare, *J. Appl. Polym. Sci.*, 2010, **102**, 1445–1451.
18 H. Sadeghifar, R. Venditti, J. Jur, R. E. Gorga and J. J. Pawlak, *ACS Sustainable Chem. Eng.*, 2016, **5**, 625–631.
19 H. Du, C. Liu, M. Zhang, Q. Kong, B. Li and M. Xian, *Progr. Chem.*, 2018, **30**(4), 448–462.
20 Y. Li, Y. Liu, W. Chen, Q. Wang, Y. Liu, J. Li and H. Yu, *Green Chem.*, 2016, **18**, 1010–1018.
21 D. Meier, V. Zúñiga-Partida, F. Ramírez-Cano, N. C. Hahn and O. Faix, *Bioresour. Technol.*, 1994, **49**, 121–128.
22 H. Du, C. Liu, Y. Zhang, G. Yu, C. Si and B. Li, *Ind. Crops Prod.*, 2016, **94**, 736–745.
23 C. Liu, B. Li, H. Du, D. Lv, Y. Zhang, G. Yu, X. Mu and H. Peng, *Carbohydr. Polym.*, 2016, **151**, 716–724.
24 X. Yang, K. Lu, K. McGrouther, L. Che, G. Hu, Q. Wang, X. Liu, L. Shen, H. Huang, Z. Ye and H. Wang, *J. Soils Sediments*, 2017, **17**, 751–762.
25 C. Liu, B. Li, H. Du, D. Lv, Y. Zhang, G. Yu, X. Mu and H. Peng, *Carbohydr. Polym.*, 2016, **151**, 716–724.
26 A. Sluiter, R. R. B. Hames, C. Scarlata, J. Sluiter, D. Templeton and D. Crocker, in *Determination of structural carbohydrates and lignin in biomass*, National Renewable Energy Laboratory, U.S. Department of Energy, 2012, NREL/TP-510-42618.

27 B. Deepa, E. Abraham, N. Cordeiro, M. Mozetic, A. P. Mathew, K. Oksman, M. Faria, S. Thomas and L. A. Pothan, *Cellulose*, 2015, **22**, 1075–1090.
28 D. Li, J. Henschen and M. Ek, *Green Chem.*, 2017, **19**, 5564–5567.
29 J. A. Sirviö and M. Visanko, *J. Mater. Chem. A*, 2017, **5**, 21828–21835.
30 M. S. Jahan, D. A. Chowdhury, M. K. Islam and S. M. Moeiz, *Bioresour. Technol.*, 2007, **98**, 465–469.
31 H. S. Du, C. Liu, X. D. Mu, W. B. Gong, D. Lv, Y. M. Hong, C. L. Si and B. Li, *Cellulose*, 2016, **23**, 2389–2407.
32 M. Smyth, A. García, C. Rader, E. J. Foster and J. Bras, *Ind. Crops Prod.*, 2017, **108**, 257–266.
33 G. Yu, B. Li, C. Liu, Y. Zhang, H. Wang and X. Mu, *Ind. Crops Prod.*, 2013, **50**, 750–757.
34 C. J. Chirayil, J. Joy, L. Mathew, M. Mozetic, J. Koetz and S. Thomas, *Ind. Crops Prod.*, 2014, **59**, 27–34.
35 R. J. Moon, A. Martini, J. Nairn, J. Simonsen and J. Youngblood, *Chem. Soc. Rev.*, 2011, **40**, 3941–3994.
36 X. Xu, F. Liu, L. Jiang, J. Y. Zhu, D. Haagenson and D. P. Wiesenborn, *ACS Appl. Mater. Interfaces*, 2013, **5**, 2999–3009.
37 H. S. Du, C. Liu, Y. D. Zhang, G. Yu, C. L. Si and B. Li, *Ind. Crops Prod.*, 2016, **94**, 736–745.
38 X. Zhou, X. Lin, K. L. White, S. Lin, H. Wu, S. Cao, L. Huang and L. Chen, *Cellulose*, 2016, **23**, 811–821.
39 Y. Wan, F. An, P. Zhou, Y. Li, Y. Liu, C. Lu and H. Chen, *Chem. Commun.*, 2017, **53**, 3595–3597.
40 A. N. Shebani, A. J. van Reenen and M. Meincken, *Thermochim. Acta*, 2008, **471**, 43–50.
41 S. S. Nair and N. Yan, *Cellulose*, 2015, **22**, 3137–3150.
42 K. Saelee, N. Yingkamhaeng, T. Nimchua and P. Sukyai, *Ind. Crops Prod.*, 2016, **82**, 149–160.
43 E. Abraham, B. Deepa, L. A. Pothan, M. Jacob, S. Thomas, U. Cvelbar and R. Anandjiwala, *Carbohydr. Polym.*, 2011, **86**, 1468–1475.
44 H. Zhu, S. Zhu, Z. Jia, S. Parvinian, Y. Li, O. Vaaland, L. Hu and T. Li, *Proc. Natl. Acad. Sci. U. S. A.*, 2015, **112**, 8971–8976.
45 K. Shahzadi, X. Zhang, I. Mohsin, X. Ge, Y. Jiang, H. Peng, H. Liu, H. Li and X. Mu, *ACS Nano*, 2017, **11**, 5717–5725.
46 B. S. Santucci, J. Bras, M. N. Belgacem, A. A. d. S. Curvelo and M. T. B. Pimenta, *Ind. Crops Prod.*, 2016, **91**, 238–248.
47 Q. Tarrés, S. Boufi, P. Mutjé and M. Delgado-Aguilar, *Cellulose*, 2017, **24**, 3943–3954.
48 J. Guo, K. M. A. Uddin, K. Mihhels, W. Fang, P. Laaksonen, J. Y. Zhu and O. J. Rojas, *ACS Sustainable Chem. Eng.*, 2017, **5**, 6978–6985.
49 H. Sehaqui, S. Morimune, T. Nishino and L. A. Berglund, *Biomacromolecules*, 2012, **13**, 3661–3667.
50 M. Henriksson and L. A. Berglund, *J. Appl. Polym. Sci.*, 2007, **106**, 2817–2824.
51 X. Kang, P. Sun, S. Kuga, C. Wang, Y. Zhao, M. Wu and Y. Huang, *ACS Sustainable Chem. Eng.*, 2017, **5**, 2529–2534.
52 H. Sehaqui, Q. Zhou, O. Ikkala and L. A. Berglund, *Biomacromolecules*, 2011, **12**, 3638–3644.
53 S. J. Chun, S. Y. Lee, G. H. Doh, S. Lee and J. H. Kim, *J. Ind. Eng. Chem.*, 2011, **17**, 521–526.
54 F. Jiang, T. Kondo and Y.-L. Hsieh, *ACS Sustainable Chem. Eng.*, 2016, **4**, 1697–1706.
55 M. Henriksson, L. A. Berglund, P. Isaksson, T. Lindstrom and T. Nishino, *Biomacromolecules*, 2008, **9**, 1579–1585.
56 A. J. Svagan, M. A. S. A. Samir and L. A. Berglund, *Biomacromolecules*, 2007, **8**, 2556–2563.
57 L. Shuai, Q. Yang, J. Y. Zhu, F. C. Lu, P. J. Weimer, J. Ralph and X. J. Pan, *Bioresour. Technol.*, 2010, **101**, 3106–3114.
58 H. Bian, L. Chen, H. Dai and J. Y. Zhu, *Carbohydr. Polym.*, 2017, **167**, 167–176.
59 J. Y. Zhu, X. J. Pan, G. S. Wang and R. Gleisner, *Bioresour. Technol.*, 2009, **100**, 2411–2418.
60 R. Bardet, C. Reverdy, N. Belgacem, I. Leirset, K. Syverud, M. Bardet and J. Bras, *Cellulose*, 2015, **22**, 1227–1241.
61 K. L. Spence, R. A. Venditti, O. J. Rojas, Y. Habibi and J. J. Pawlak, *Cellulose*, 2011, **18**, 1097–1111.
62 Y. Feng, J. Zhang, J. He and J. Zhang, *Carbohydr. Polym.*, 2016, **147**, 171–177.
63 Y. Deng, X. Feng, M. Zhou, Y. Qian, H. Yu and X. Qiu, *Biomacromolecules*, 2011, **12**, 1116–1125.
64 D. B. Mahadik, R. V. Lakshmi and H. C. Barshilia, *Sol. Energy Mater. Sol. Cells*, 2015, **140**, 61–68.

